AIMS Materials Science, 6(4): 498–508.
DOI: 10.3934/matersci.2019.4.498
Received: 27 February 2019
Accepted: 21 May 2019
Published: 21 June 2019

http://www.aimspress.com/journal/Materials

Research article

The effect of the surface roughness and ageing characteristics of boehmite on the removal of biological particles from aqueous solution

Leonid A. Kaledin*, Fred Tepper, Yuly Vesga and Tatiana G. Kaledin

Department of Nanotechnology and Filtration, Argonide Corporation, 291 Power Court, Sanford, FL 32771, USA

* **Correspondence:** Email: kaledin@argonide.com; Tel: +14073222500; Fax: +14073221144.

Abstract: Two-dimensional (2D) and one-dimensional (1D) quantum-sized γ-AlOOH structures were deposited onto siliceous and cellulosic substrates in a one-step, aqueous, and moderate temperature process. Low cost, large scale manufacturing of siliceous and cellulosic substrates coated with 2D and 1D arrays of γ-AlOOH crystallites of 2.7 ± 0.5 nm in diameter, with an average height of 3 ± 2 nm and 250 ± 50 nm, respectively was demonstrated. Direct measurement of streaming potentials in NaCl aqueous electrolyte was accomplished in order to characterize the zeta potentials of the as mentioned surfaces. It was shown that the isoelectric point value of rough nanostructured surface is three pH units higher as compare to the flat crystalline γ-AlOOH surface, resulting in a high removal efficacy of submicron particles from aqueous suspension by the surfaces with combined microscale and nanoscale structures. Furthermore, ageing characteristics of the 2D and 1D γ-AlOOH crystallites were presented, which showed great removal efficiencies after seven to fourteen years of manufacturing.

Keywords: two-dimensional (2D); one-dimensional (1D); point of zero charge (PZC); isoelectric point (IEP); zeta potential; electrical double layer (EDL); electrokinetic phenomena (EKP)

1. Introduction

Coating sand and diatomaceous earth particles with aluminum oxyhydroxide changes the zeta potential of filtration media from negative to positive in a pH range from 3 to 11 [1] due to the fact that it modifies the surface properties of the filter media by coating it with an electropositive material [2–7]. As an alternative, aluminum hydroxides have been used for treatment of water to

reverse the surface charge on microorganisms, facilitating their coagulation and flocculation [8]. For this reason, media such as coated sand and diatomaceous earth have been showed to improve removal efficacy of submicron particles, i.e., viruses and bacteria [1–7]. In spite of some success in describing better removal efficacy of submicron particles by electropositive media, a fundamental understanding of why deposition is improved to a greater degree in some coatings is missing [4].

The role of the electrical double layer (EDL) and van der Waals forces in particle deposition is often viewed in terms of Derjaguin-Landau-Verwey-Overbeek (DLVO) theory [9,10], which was developed for smooth, homogeneous particles with ideal geometries and with no DL overlap. The influence of surface roughness of filter media on streaming potential measurements is well documented [11]. The samples made from the same material with different surface roughness, measured by the same method, in the same device showed zeta potential values significantly different from each other, while the isoelectric point (IEP) values were identical between the measurements [11]. Moreover, the velocity profiles for two different spots along the surface of a multifilament fabric showed circulation pattern between two yarns during the streaming potential measurement. The general impact of roughness is to amplify the long-range behaviour of noncontact DLVO forces with the approximate amplification factor of exponential force between rough and smooth surfaces ($\sigma_{roughness}^2/\lambda_{Debye}^2$), where $\sigma_{roughness}$ is the mean roughness [12]. Furthermore, the influence of particle shape and particle size on the zeta potential of colloidal suspensions is well known for the case of ultrapure silica powders where the authors found that the maximum zeta potential occurs for particle size ranging between 100 nm and 1 μm [13].

A variety of analytical and numerical models have been developed to describe the pressure-driven flow over heterogeneous surfaces. The vast majority of these models assume that the local EDL field is independent of the flow field [14–17]. However, for pressure-driven flow over a surface with heterogeneous patches, the local EDL fields are not uniform. This means that they are more different above a patch than in the region between the patches. This irregularity produces distortions in the equilibrium electrostatic field. Consequently, the electrostatic potential can alter the value of the zeta potential from its expected value over a surface with uniformly smeared surface under conditions of moderate surface charge [18–21]. The characteristic symptom of field distortion is the generation of flow velocities in all three coordinate directions, including a circulation pattern perpendicular to the main flow axis.

One of the purposes of this paper is to investigate the effect of nanoscale surface roughness on filtration of micron and sub-micron biological particles from aqueous solution by 2D and 1D γ-AlOOH-coated siliceous and cellulosic particles associated with pressure-driven flow through a 3-mm deep precoat and through a non-woven filter media [5–7]. The other one is to present the great ageing characteristics of the 2D and 1D γ-AlOOH crystallites, which showed no degradation in performance (i.e., TEM and XRD patterns, particle size distribution, etc.) over periods of seven and fourteen years, respectively. This is a very important finding since a large-scale manufacturing of siliceous and cellulosic substrates coated with 2D and 1D arrays are being proposed. The 1D filter media is manufactured and sold as non-woven media by Ahlstrom Filtration LLC under the tradename Disruptor™. The 2D filter aid media is manufactured by Argonide Corporation in large scale processes.

2. Materials and method

2.1. Synthesis of 2D quantum-sized and 1D nanometer-sized γ-AlOOH crystals adhered to siliceous and cellulosic substrates

Synthesis of 2D quantum-sized and 1D nanometer-sized γ-AlOOH crystals adhered to siliceous and cellulosic substrates with BET (Brunauer, Emmett, Teller) specific surface area from 3 to 80 m^2/g was accomplished via a reaction of aluminum powder with alkaline water [5–7]:

$$2Al\ (s) + 4H_2O\ (l) \rightarrow 2AlOOH\ (s) + 3H_2\ (g) \quad (1)$$

The step-by step descriptions of the 2D quantum-sized γ-AlOOH crystals synthesis adhered to siliceous substrate were initially reported in reference [7]. The siliceous powder, in form of diatomaceous earth was dispersed in 4 liters of RO water and allowed to react with 17.5 g of micron size aluminum powders in the presence of 40 mL of 10 M NaOH at ambient pressure. It was heated to boiling point while mixing with an air-driven mixer at 300 rpm. Then, the suspension was cooled down to 40–50 °C and neutralized to pH 6–8 with 10% sulfuric acid. Decantation was allowed. Then, it was dried overnight at 100 °C. Finally, the media was crushed and sieved through a 170-mesh sieve. The synthesis of one-dimensional (1D) nanometer-sized γ-AlOOH atomic crystals adhered to siliceous and cellulosic substrates was accomplished via the same Eq 1 of aluminum powder with alkaline water [5]. Amounts of 0.5 g of aluminum metal powder and 1.5 g of amorphous borosilicate glass microfiber with average diameter of 0.6 μm were dispersed in 0.5 L liter of RO water and were reacted in a 1 L stainless steel pot in the presence of 1 mL of 10 M NaOH at ambient pressure. The suspension was heated to its boiling point at ambient pressure while mixing with an air-driven mixer equipped with 5 cm diameter impeller at 300 rpm. The suspension was cooled down to 40–50 °C, neutralized with 10% sulfuric acid to pH 6–8. The non-woven paper-like mat was formed by conventional wet-laid paper making technology. Nitrogen BET specific surface area of dry sample of γ-AlOOH nanofibers 2.7 ± 0.5 nm in diameter and 250 ± 50 nm long (Figure 1a) was $S_{BET}^{\gamma-\mathrm{AlOOH}}$ = 475 m^2/g [5]. Nitrogen BET surface area of dry samples of microglass fibers with an average diameter of 0.6 μm [5] (see Figure 1c) increased by approximately 50 times from $S_{BET}^{fiber,d\,=\,0.6\,\mu m}$ = 3 m^2/g to $S_{BET}^{\gamma-\mathrm{AlOOH}/fiber}$ = 150–200 m^2/g and in the case of lyocell cellulosic fibers [6] (see Figure 1b) the BET value increased by a factor of two from estimated value of $S_{BET}^{fiber,d=0.05\,\mu m}$ = 80 m^2/g to estimated value of $S_{BET}^{\gamma-\mathrm{AlOOH}/fiber}$ = 150–200 m^2/g. This suggests formation of additional surfaces on the substrates as seen in Figure 1b,c.

2.2. Transmission electron microscopy (TEM)

The TEM images (Figure 1a,c) were recorded on the JEOL JEM2010 TEM at 200 kV accelerating voltage. The high resolution TEM (HRTEM) images (Figure 1d) were recorded on the Tecnai F30 at 300 kV accelerating voltage.

3. Results and discussion

3.1. TEM analysis

Representative samples of 2D and 1D materials obtained by the procedures described previously [5–7] were investigated further by TEM and HRTEM. In Figure 1a, γ-AlOOH nanofibers 2.7 ± 0.5 nm in diameter and 250 ± 50 nm long are presented. Figure 1b,c shows examples of the TEM images of the 1D γ-AlOOH crystallites, 2–3 nm in diameter and approximately l = 250 nm long that are electroadhesively grafted via van der Waals (VDW)-type interlayer bonds to a 50 nm diameter cellulosic lyocell nanofiber and to a 0.6 μm glass microfiber, respectively [6]. Figure 1d shows an example of the atomic-resolution HRTEM image of 2D γ-AlOOH crystallites grafted via VDW type interlayer bonds to a 5 μm diameter diatomaceous earth (DE) particle. Thickness of the 2D γ-AlOOH crystallites was estimated to be in the range from 1 to 5 nm based on a HRTEM image of the DE particle edge (Figure 1d).

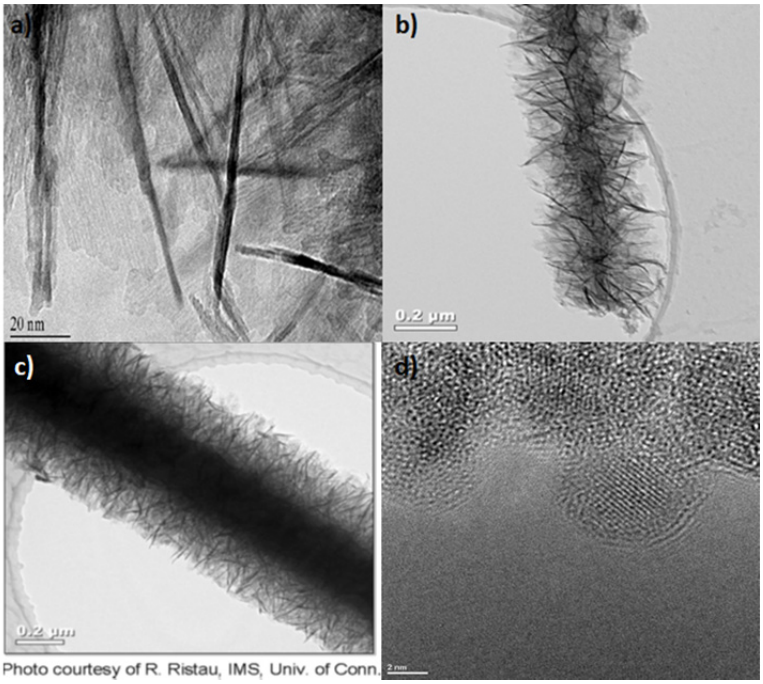

Figure 1. TEM characterization of 2D and 1D γ-AlOOH crystallites: (a) TEM image of the 1D γ-AlOOH crystallites [5], (b) TEM image of the 1D γ-AlOOH crystallites attached to a 50 nm diameter lyocell cellulosic fiber [6], (c) TEM image of the 1D γ-AlOOH crystallites attached to a 0.6 μm diameter glass microfiber [5] and (d) HRTEM image of the 2D γ-AlOOH crystallites attached to a 5 μm diameter DE particle [7] with atomic resolution.

Figure 2 shows a sketch of the 2D γ-AlOOH crystallites deposited onto siliceous substrate. When the lateral dimensions of 2D structures are approximated by a circle, they are 7–10 times greater than the boehmite a–c unit cell dimensions. This is consistent with boehmite crystal growth, which occurs mainly along the a–c plane where atomic in-plane bonds are stronger than the weak,

VDW type, interlayer bonds along the *b*-axis [22]. Assuming that the crystals seen in Figure 1d are fully dense γ-AlOOH cylinders (Figure 2) with diameter (d), length (l), silica surface fraction coverage (θ) with nitrogen BET specific surface area values of $S_{BET}^{DE,\ APS=5\ \mu m}$ = 51 m^2/g and $S_{BET}^{\gamma-\mathrm{AlOOH}/DE}$ = 69 m^2/g, the ratio l/d = 1.2 ± 0.7 translates into l = 3 ± 2 nm. This implies that the average height (length l) of the 2D γ-AlOOH crystals seen in Figure 1d is comparable to the boehmite cell dimension b = 12 Å [22].

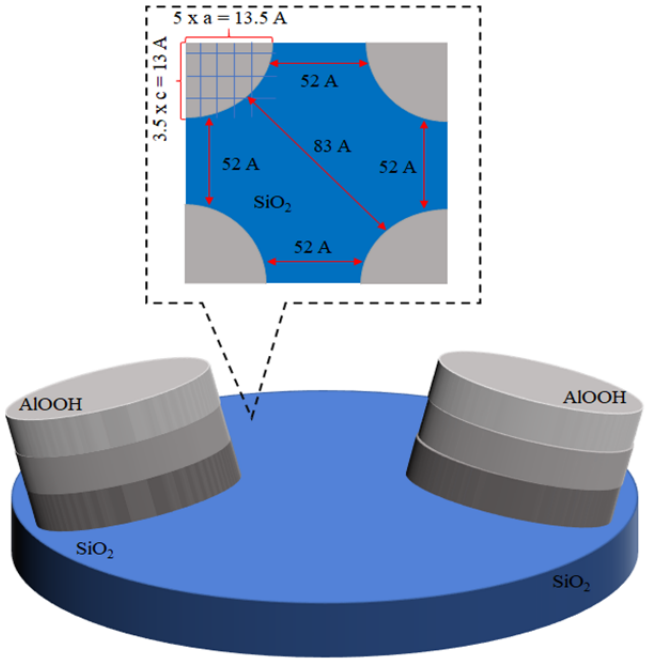

Figure 2. Sketch of 2D γ-AlOOH crystallites deposited onto siliceous substrate.

3.2. Zeta potentials of aluminized 2D and 1D γ-AlOOH/siliceous particles

It was found that aluminized 2D and 1D γ-AlOOH /siliceous particles are highly electropositive in aqueous solution with zeta potential $\zeta \geq 40$ mV [23] at γ-AlOOH loading greater than 15 weight percent (wt%) as compared to the highly electronegative character of the bare siliceous substrates ($\zeta \leq -70$ mV, Figure 3). The point of zero charge (PZC) of aluminized γ-AlOOH siliceous particles was determined to be 11.6 ± 0.2 for 1D and 11.4 ± 0.2 for 2D structures, respectively [23]. This is three pH units higher as compare to the flat crystalline γ-AlOOH surface. Borghi et al. [24] observed a remarkable reduction by several pH units of the isoelectric point (IEP) on rough nanostructured surfaces, with respect to flat crystalline rutile TiO_2. In order to explain the observed behavior of IEP, Borghi et al. [24] considered the roughness-induced self-overlap of the electrical double layers as a potential source of deviation from the trend expected for flat surfaces. Contrary to the acidic behavior of nanostructured surfaces crystalline rutile (Lewis acid sites), aluminized surfaces of siliceous particles with quantum size 2D and 1D γ-AlOOH behave preferentially as *basic loci* [23].

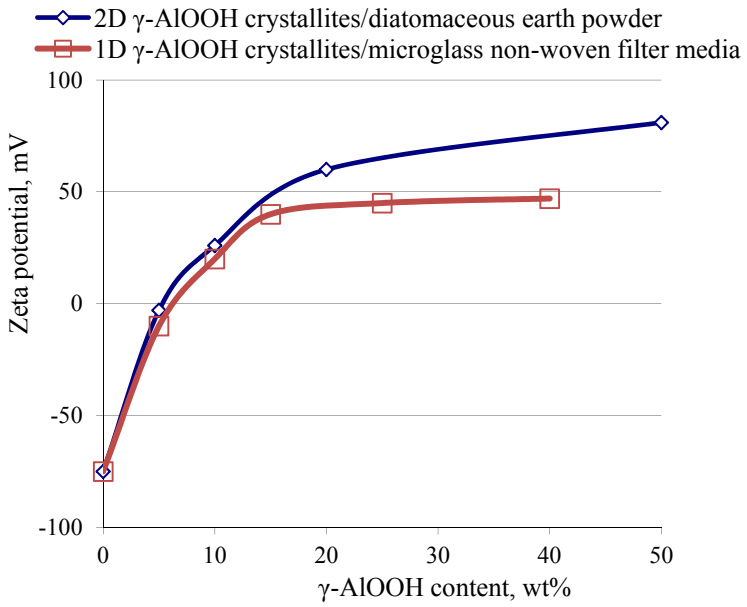

Figure 3. Zeta potential of 2D and 1D γ-AlOOH crystallites deposited onto siliceous substrates as a function of γ-AlOOH loading.

3.3. Removal efficacy of submicron particles as a function of pH and electrolyte ionic strength

Table 1 shows initial removal efficacy of biological particles from aqueous solution associated with pressure-driven flow through micrometer size pores of either 2D γ-AlOOH/DE particles packed into a 3-mm deep precoat [25] or through a 1D γ-AlOOH/microglass non-woven filter media [5,6]. A striking feature of Table 1 is that 2D and 1D structures result in a high removal efficacy (in all cases greater than 99.9%) of biological particles regardless of zeta potential value in the range from 15 mV to 56 mV. Estimations show that Brownian displacement does not play significant role in removal efficacy of submicron size RT bacteria in a 3-mm deep γ-AlOOH/DE precoat with mean flow pore size of $d_{\text{mean-flow}} = 24 \pm 4$ μm for aluminized DE with average particle size of 80 μm [1]. When the Stokes-Einstein equation [26] is applied to a spherical particle suspended in water, it produces an estimated root-mean-square displacement during a contact time of 4.5 s in a 3-mm deep precoat of only 1.8 μm in the case of RT bacteria. Furthermore, the electrostatic attraction should not play significant role due to highly efficient shielding by the EDL layer with Debye length as short as 1.6 Å in the case of RT suspension in the 3.4 M NaCl electrolyte (Table 1). Anisotropic characteristics of EDL layer have been observed in numerous material systems. Charging behavior of the EDL layer has been studied for various metal oxide/hydroxide surfaces in aqueous solutions [24,27–29]. Van Olphen has shown a pH-dependent charge at the edges and faces of kaolinite platelets [30] and concluded that the double-layer structure is complicated by the fact that two crystallographically different surfaces are carrying a different type of double layers that under certain condition can have opposite signs. Recent measurements of the EDL properties of CaF_2 [27], α-Al_2O_3 (Sapphire) [28], TiO_2 (Rutile) [24,29] indicated significant differences (up to 2 pH units) between the isoelectric points in various crystallographic orientations of surfaces.

Table 1. Initial removal efficacy of bioparticles as a function of pH and electrolyte ionic strength.

Material	Zeta potential (mV)	pH	Electrolyte ionic strength (mM)	λ_D[a] (nm)	RT removal efficacy (LRV)	MS2 removal efficacy (LRV)
γ-AlOOH/glass[b]	47 ± 9	7.0	0.002(1)	215	>7.0	5.1
γ-AlOOH/DE[c]	56 ± 9				>7.0	6.3
γ-AlOOH/glass[b]	47 ± 9		3400	0.16	7.7[d]	3.8[d]
γ-AlOOH/DE[c]	56 ± 9				>7.1	5.3
γ-AlOOH/glass[b]	23 ± 6	10.5	0.33(3)[e]	17	>6.9	7.4
γ-AlOOH/DE[c]	15 ± 3				>4.5	3.1
γ-AlOOH/glass[b]	23 ± 6		3400	0.16	7.7[d]	3.8[d]
γ-AlOOH/DE[c]	15 ± 3				5.5	4.0

*Note: (a) For NaCl electrolyte with bulk concentration c_{NaCl} at T = 25 °C the Debye length equals to $\lambda_D \cong 0.304/\sqrt{c_{NaCl}}$ (in nm) where c_{NaCl} is the concentration of the salt, in mol/dm^3, (b) non-woven γ-AlOOH media, (c) 3-mm γ-AlOOH/DE precoat, (d) by 2 layers of non-woven γ-AlOOH media and (e) elevated due to pH adjustment with NaOH.

3.4. Removal efficacy of bio particles by a mixture of opposively charged particles

In this section, we will discuss the 3D flow structure associated with pressure-driven flow through micrometer size pores of a mixture of equal but opposite charged particles packed into a 3-mm deep precoat [25]. The surfaces of DE and aluminized γ-AlOOH/DE have similar but opposite values of zeta potentials (Figure 3). In such a case, there is an excess of positive ions over the DE surface, but negative ions dominate over the aluminized DE surface to balance out the positive surface charge. The difference in the surface potential results in an electrostatic potential gradient within the local electrical double layer (EDL) fields near the transition zone between the two regions. The presence of this potential gradient results in a body force on the microbes and/or ions in the double layer; however, in this case, an opposite body force is applied to the negative ions over the positively charged particle. As a result, the net body force over the region is zero and the circulation velocity perpendicular to the main flow becomes negligible [18–21]. The aluminized γ-AlOOH/DE and DE particles have equal average size of d = 80 ± 3 μm. It was assumed to be packed in simple cubic cell with particles only at the corners as seen in Figure 4a,b. DE particles were mixed with aluminized γ-AlOOH/DE particles with DE content in the mix of 10-, 25-, 50-, and 75-wt% and formed a 3-mm deep precoats ($\Delta_{\text{thickness}}$ = 3 mm). Assuming a simple cubic cell packing, the number of layers is estimated as $N_{\text{layers}} = \Delta_{\text{thickness}}/d_{\text{average}} \sim 38$.

Table 2 shows removal efficacy of MS2 bacteriophages and RT bacteria by a 3 mm precoats of aluminized γ-AlOOH/DE80 and DE80 mix at a flow velocity of 0.67 mm/s, neutral pH 7 and ionic strength of 2 ± 1 μM. The mean flow pore diameter of the precoat layer was determined to be 24 ± 5 μm [1]. Results in Table 2 provides experimental evidence of a behavior when a 3 mm precoat is losing adsorption properties of the aluminized γ-AlOOH/DE tested in the same configuration at much faster rate than one can expect based on the weight fraction of DE in the mix. For example, for a 50/50-wt% mix one can expect a reduction in adsorption efficacy by a factor of two or by $\log_{10}(1/2) = -0.3$ based on weight percent of the aluminized γ-AlOOH/DE fraction in the mix while

experimental reductions are 3.5 ± 1.0 LRV for MS2 and greater than 4.7 LRV for RT bacteria (Table 2). This is consistent with the case when at least one of the neighboring particles on the side of the cube perpendicular to the flow direction has opposite sign of the surface charge, i.e., $-|\sigma_2|$ for DE than the other neighboring particles, i.e., $+|\sigma_1|$ for aluminized γ-AlOOH/DE ceasing the circulation pattern in that pore involving four neighboring particles. That is, one DE particle is cancelling out high removal efficacy of three aluminized γ-AlOOH/DE particles situated on the same side of the cube perpendicular to the flow direction (Figure 4b).

The average number of layers in a pore formed by a group of four aluminized DE particles with no DE particle in the group decreased rapidly as DE loadings in the mix increases. Table 2 presents average number of layers in a pore formed by a group of four aluminized DE particles with no DE particle in the group together with the average layer thickness in the 3-mm precoat formed by four neighboring aluminized DE particles with no DE particle in the group.

Table 2. Removal efficacy of MS2 and RT by a mixture of equal size but opposively charged aluminized γ-AlOOH/DE and DE particles.

DE in aluminized γ-AlOOH/DE and DE mix precoat (%)	Average number of layers formed by four neighboring aluminized γ-AlOOH/DE particles	Average layer thickness formed by four neighboring aluminized γ-AlOOH/DE particles (mm)	MS2 removal efficacy (LRV)	RT removal efficacy (LRV)
0	38	3.00	6.1 ± 0.1	>7.7
10	29	2.28	5.1 ± 0.2	6.7 ± 0.5
25	13	1.02	3.6 ± 0.4	3.9 ± 0.3
50	5	0.38	2.6 ± 0.9	3.0 ± 0.3
75	1	0.11	1.0 ± 0.2	2.2 ± 0.1
100	0	0.00	0.5 ± 0.1	0.7 ± 0.2

3.5. Flow mixing via electrokinetic circulation

Electrokinetic phenomena are typically second-order phenomena, e.g., in streaming current measurements, an applied mechanical force produces an electric current [14]. When treated phenomenologically, the second order phenomena can be treated by irreversible thermodynamics [15]. Classical thermodynamics describes EDL at rest, while in electrokinetics EDL is not at rest although usually the deviations from the equilibrium distribution of charge are disregarded [15].

Figure 4 shows removal efficacy of MS2 bacteriophages and RT bacteria by 3-mm deep precoat of aluminized γ-AlOOH/DE80 and DEAL80 mix as a function of average layer thickness formed by four neighboring aluminized γ-AlOOH/DE particles. Figure 4 also reveals good correlation (coefficient of determination $R^2 > 0.99$) between LRV values of microbial removal efficacy and average layer thickness formed by four neighboring aluminized γ-AlOOH/DE (Table 2):

$$\log_{10}(C_{initial}/C_{filtrate}) = x/x_0 + a \quad (2)$$

where a is a constant and x_0 is the average thickness of aluminized γ-AlOOH/DE layer within a mix that would reduce the initial concentration, $C_{initial}$, by a factor of 10. The thickness of aluminized γ-AlOOH/DE precoat layer that would reduce concentration of biological particles in the water stream by a factor of 10 is equal to x_0(MS2) = 0.8 mm for MS2 bacteriophage and x_0(RT) = 0.5 mm for RT bacteria.

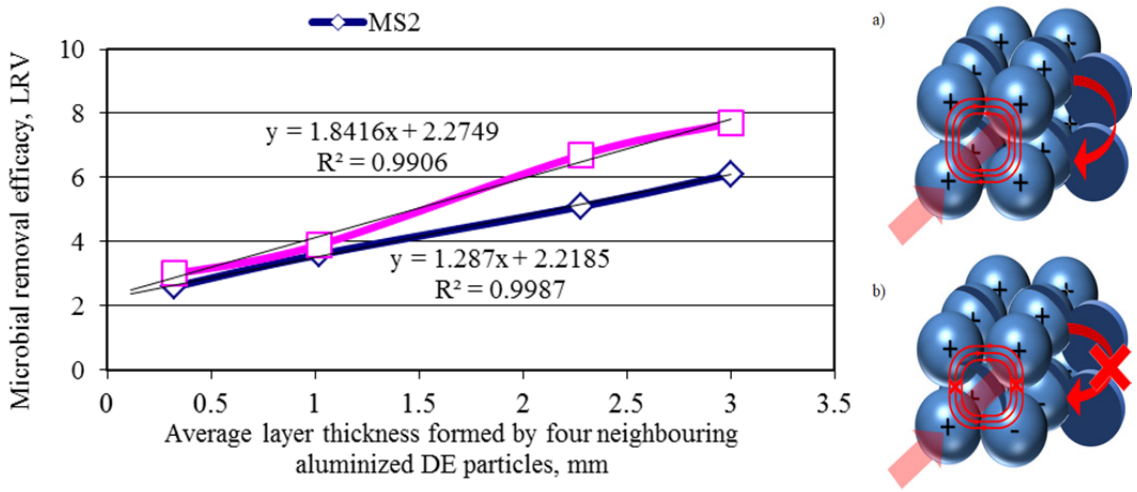

Figure 4. Removal efficacy of MS2 bacteriophages and RT bacteria by 3-mm deep precoat made from a mixture of γ-AlOOH/DE and DE particles. (a) and (b) diagram showing net surface charge density and velocity vector contours in the double layer region for the close cubic cell packing of: (a) γ-AlOOH/DE particles; (b) mixture of γ-AlOOH/DE and DE particles.

3.6. Ageing characteristics of the 2D and 1D γ-AlOOH crystallites

The main application of the prepared 2D and 1D γ-AlOOH crystallites is as water purification media. Additionally, since we are proposing a low cost and large-scale production of these crystallites, it was important to know their stability throughout the time. For this reason, the removal efficacy of aqueous particles suspended by the prepared 2D and 1D γ-AlOOH crystallites was evaluated after seven and fourteen years, respectively.

From the results presented in Table 3, it was found that the prepared 2D and 1D γ-AlOOH crystallites remain monocrystalline under ambient conditions and no degradation in performance (i.e., TEM and XRD patterns, particle size distribution, etc.) was noticed over periods of several years. Table 3 shows the performance of the media to remove biological particles from aqueous solution after seven to fourteen years of manufacturing. This finding makes the crystallites to be industrially applicable.

Table 3. Initial removal efficacy of bioparticles at neutral pH as a function of ageing.

Material	Ageing time	RT removal efficacy[a] (LRV)	MS2 removal efficacy[a] (LRV)
–AlOOH/glass	As produced	>6.5	>7.0
	Aged for 14 years	>7.0	>7.3
–AlOOH/DE[b]	As produced	>7.3	>7.0
	Aged for 7 years	>7.3	>6.2

*Note: (a) average of 5 replicates and (b) DE with average particle size of 18 μm.

4. Conclusions

In conclusion, aluminum-water reaction (Eq 1) has successfully been used to produce 2D and 1D quantum-sized γ-AlOOH structures deposited onto siliceous and cellulosic substrates in a one-step process at moderate temperature [5–7]. Low cost, large scale manufacturing (several metric tons per year) of siliceous and cellulosic substrates coated with 2D and 1D arrays of γ-AlOOH crystallites was demonstrated. The efficacy for removal of biological particles was improved by increasing the surface roughness of the material. Finally, the prepared 2D and 1D γ-AlOOH crystallites remain monocrystalline under ambient conditions and no degradation in performance (i.e., TEM and XRD patterns, particle size distribution, etc.) was noticed over periods of several years (i.e., seven to fourteen years).

Conflict of interests

No potential conflict of interest was reported by the authors.

References

1. Kaledin L, Tepper F, Kaledin T (2017) Electrokinetic aspects of water filtration by AlOOH-coated siliceous particles with nanoscale roughness. *AIMS Mater Sci* 4: 470–486.
2. Farrah S, Preston D (1985) Concentration of viruses from water by using cellulose filters modified by *in situ* precipitation of ferric and aluminum hydroxides. *Appl Environ Microb* 50: 1502–1504.
3. Lukasik J, Farrah S, Truesdail S, et al. (1996) Adsorption of microorganisms to sand and diatomaceous earth particles coated with metallic hydroxides. *Kona Powder Part J* 14: 87–91.
4. Truesdail S, Lukasik J, Farrah S, et al. (1998) Analysis of bacterial deposition on metal (hydr)oxide-coated sand filter media. *J Colloid Interf Sci* 203: 369–378.
5. Tepper F, Kaledin L (2005) Nanosize electropositive fibrous adsorbent. US Patent 6,838,005.
6. Tepper F, Kaledin L (2008) Drinking water filtration device. US Patent 7,390,343.
7. Kaledin L, Tepper F, Kaledin T (2016) Aluminized silicious powder and water purification device incorporating the same. US Patent 9,309,131.
8. Clesceri L, Greenberg A, Eaton A (1998) *Standard Methods for Examination of Water and Wastewater*, Washington, DC: American Public Health Association.
9. Derjaguin B, Landau L (1993) Theory of stability of strongly charged lyophobic sols of the adhesion of strongly charge particles in solution electrolytes. *Prog Surf Sci* 43: 30–59.
10. Verwey E, Overbeek J (1948) *Theory of the Stability of Lyophobic Colloids*, Amsterdam: Elsevier.
11. Schnitzer C, Ripperger S (2008) Influence of surface roughness on streaming potential method. *Chem Eng Technol* 31: 1696–1700.
12. Parsons D, Walsh R, Craig V (2014) Surface forces: surface roughness in theory and experiment. *J Chem Phys* 140: 164701.

13. Seeger S, Palm B, Günster J, et al. (2015) On the influence of the particle size on the zeta potential of ultra-pure silica powders. *Ber DKG* 92: E35–E40. Available from: https://www.tib.eu/en/search/id/tema%3ATEMA20150904226/On-the-Influence-of-the-Particle-Size-on-the-Zeta/#documentinfo.
14. Lyklema J (1995) *Fundamentals of interface and colloid science. Volume II: Solid-Liquid Interfaces*, Academic Press.
15. Lyklema J (1991) *Fundamentals of interface and colloid science. Volume I: Fundamentals*, Academic Press.
16. Lyklema J (2003) Electrokinetics after Smoluchowski. *Colloid Surface A* 222: 5–14.
17. Hunter R (2001) *Foundations of Colloid Science*, Oxford: Oxford University Press.
18. Cohen R, Radke C (1991) Streaming potentials of nonuniformly charged surfaces. *J Colloid Interf Sci* 141: 338–347.
19. Li D (2004) *Electrokinetics in Microfluidics*, Amsterdam: Elsevier Academic Press.
20. Erickson D, Li D (2002) Microchannel flow with patchwise and periodic surface heterogeneity. *Langmuir* 18: 8949–8959.
21. Erickson D, Li D (2001) Streaming potential and streaming current methods for characterizing heterogeneous solid surfaces. *J Colloid Interf Sci* 237: 283–289.
22. Bokhimi X, Toledo-Antonio J, Guzman-Castillo M, et al. (2001) Relationship between crystallite size and bond lengths in boehmite. *J Solid State Chem* 159: 32–40.
23. Kaledin L, Tepper F, Kaledin T (2016) Pristine point of zero charge (p.p.z.c.) and zeta potentials of boehmite's nanolayer and nanofiber surfaces. *Int J Smart Nano Mater* 7: 1–21.
24. Borghi F, Vyas V, Podesta A, et al. (2013) Nanoscale roughness and morphology affect the isoelectric point of titania surfaces. *PloS One* 8: e68655.
25. Argonide Corporation (2015) Preparation of 3-mm deep precoat from 80 μm DE powders. Available from: www.tinyurl.com/my6jmzz.
26. Einstein A (1956) *Investigations on the Theory of the Brownian Movement*, New York: Dover Publications.
27. Assemi S, Nalaskowski J, Miller J, et al. (2006) Isoelectric point of fluorite by direct force measurements using atomic force microscopy. *Langmuir* 22: 1403–1405.
28. Kershner R, Bullard J, Cima M (2004) Zeta potential orientation dependence of sapphire substrates. *Langmuir* 20: 4101–4108.
29. Bullard J, Cima M (1995) Orientation dependence of the isoelectric point of TiO_2 (Rutile) surfaces. *J Phys Chem* 99: 2114–2118.
30. Van Olphen H (1977) *An Introduction to Clay Colloid Chemistry*, New York: John Wiley and Sons.

AIMS Press